Depolymerization of polyesters by a binuclear catalyst

Zhiqiang Niu (niuzq@tsinghua.edu.cn)
Tsinghua University https://orcid.org/0000-0002-9122-4880
Shengbo Zhang
Tsinghua University
Qikun Hu
Tsinghua University https://orcid.org/0000-0003-1607-420X
Yu-Xiao Zhang
Tsinghua University https://orcid.org/0000-0002-9112-9947
Haoyue Guo
Brookhaven National Laboratory
Yanfen Wu
Tsinghua University
Mingze Sun
Tsinghua University https://orcid.org/0000-0003-0027-0003
Xingsong Zhu
Sinopec Yizheng Chemical Fibre Co., Ltd.
Jiangang Zhang
Tsinghua University
Shuyan Gong
Tsinghua University
Ping Liu
Brookhaven National Laboratory

Article

Keywords: PET hydrolysis, environment remediation, plastic recycling, proximity effect, binuclear catalyst

Posted Date: December 29th, 2022

DOI: https://doi.org/10.21203/rs.3.rs-1360945/v1

Version of Record: A version of this preprint was published at Nature Sustainability on May 1st, 2023. See the published version at https://doi.org/10.1038/s41893-023-01118-4.

Abstract

Remediation and reuse of discarded plastics can reduce their accumulation in the environment and bring energy savings for plastic production. Here we discover a binuclear zinc catalyst that features a biomimetic intramolecular pathway for polyester depolymerization, which not merely enables environmental degradation of PET but also affords industrial-scale PET recycling under relatively mild conditions. The binuclear catalyst delivers a specific activity of 36 mg_{PET} d^{-1} g_{catal}^{-1} toward PET depolymerization at pH 8 and 40 ^{o}C, the very condition holding the possibility of naturally breaking down plastic waste. The structural stability of this synthetic catalyst allows it to work under wide operational conditions, resulting in a specific activity of 577 g_{PET} h^{-1} g_{catal}^{-1} at pH 13 and 90 ^{o}C for centralized PET recycling. A closed-loop production of bottle-grade PET was also demonstrated. Besides, this catalyst is catalytically active toward a wide scope of substrates with high tolerance to additives and impurities.

Introduction

The surge of plastic production since the 1950s is accompanied by the spread of plastics across the earth system[1–5]. Ubiquitous plastic waste imposes harmful impacts on the environment, especially on marine ecosystem[4,6]. The escalating plastic pollution calls for remediation and recycling strategies. Poly(ethylene terephthalate) (PET), the most abundantly produced polyester, accounts for nearly 12% of total solid waste[7,8]. Mechanical processing of PET waste often leads to deterioration of the material properties[9]. Chemical recycling allows to produce PET products with unchanged functionality. However, the current chemical depolymerization is often operated under harsh conditions of intense heat (>180 °C) and/or pressure (20–40 atm), caustic bases (e.g., NaOH 4–20 wt%) or acids (e.g., H_2SO_4 > 87 wt%), resulting in high energy cost and a great deal of hazardous waste[7]. Moreover, a large fraction of post-consumer PET escapes waste management system and goes into environment. Hence, it is essential to develop more efficient and environmental-friendly recycling and remediation routes to depolymerize plastics under mild or even environmental conditions.

Enzymatic depolymerization shows substantial promise in plastic recycling and environment remediation under mild conditions. Several plastic-degrading enzymes have been discovered from the habitat of microbes which have capabilities to consume plastics for metabolism[10–15]. For instance, PET can be hydrolyzed by cutinases and PETases under ambient conditions[12], a process that will appreciably occur only under harsh conditions by non-enzymatic ways[16]. The capability of PET-degrading enzymes to break down PET under mild conditions arises in part from the proximity effect[17–21], where the substrate-binding cleft brings the carbonyl and hydroxyl groups into proximity, akin to an effective increase in the local concentration of the reactants. In fact, similar strategies are employed in many other hydrolases[22–25], except that the binding clefts of PET-degrading enzymes are close to the surface of proteins, allowing access to polymeric substrates.

Translating the proximity effect of enzymatic catalysis into the structure design of synthetic plastic-degrading catalysts will help us better cope with the global plastic challenge. One strategy is to construct structural analogues or functional models for the active sites of relevant hydrolases. Mimicry of the active sites of cutinases or PETases is intimidating, as they are constituted by approximately twenty key residues with intricate and precise positioning[18]. We therefore directed our attention to metallohydrolases which have been demonstrated more feasible for biomimetic design[22]. Binuclear metallohydrolases are a wide class of enzymes that utilize two metal centers to give maximal acceleration of various hydrolytic processes via the proximity effect. One of them, organophosphate-degrading enzyme from *A. radiobacter* (OpdA) got on our radar due to its substrate promiscuity[23]. OpdA is a homobinuclear metallohydrolase whose active site consists of two metal ions (e.g., di-Zn^{2+}, di-Co^{2+}, etc.). OpdA accelerates the hydrolysis of phosphate with similar principles used by the PET-degrading enzymes despite of the superficially disparate substrates. During the reaction, phosphate and hydroxyl bind to adjacent metal centers respectively, such that the reactants are brought in close proximity, leading to increased local concentration of nucleophilic hydroxide (Fig. 1a). Meanwhile, the binding increases the electrophilicity of phosphate and stabilizes the intermediate afterwards[23–25]. So far, there is no record indicating that OpdA or other binuclear metallohydrolases have activities toward PET degradation. This is probably because their active sites are not accessible to polymers. We hypothesize that the binuclear active site of OpdA can potentially catalyze PET degradation if the surrounding scaffold is removed (Fig. 1b).

To test this hypothesis (Fig. 1b), we synthesized a Robson-type binuclear zinc catalyst. Its structure resembles the active sites of OpdA. Remarkably, the binuclear zinc catalyst can depolymerize PET at pH 8 as well as in natural seawater. Mechanistic investigations indicate that the efficient PET depolymerization over this binuclear zinc catalyst originates from an intramolecular reaction pathway, exactly matching the characteristics of binuclear hydrolases. In previous studies, Zn(II) salts or zinc oxide were widely employed as Lewis acid catalysts in PET hydrolysis or glycolysis (depolymerization by glycols)[7,9], but they showed no hydrolysis activity at pH 8 and only worked at high concentrations of alkali, suggesting the proximity effect imparted by the binuclear sites plays a critical role. This synthetic binuclear catalyst remains robust over a wide range of operational temperature (30–340 ^{o}C) and pH (8–14). As a result, a specific activity of 577 $g_{PET}\ h^{-1}\ g_{catal}^{-1}$ and a productivity of 50 $g\ L^{-1}\ h^{-1}$ of terephthalate was realized for sustainable PET recycling at pH 13 and 90 ^{o}C. We further showcased a closed-loop production of bottle-grade PET using the recycled terephthalate. This synthetic catalyst has high tolerance to various additives and impurities, and exhibits catalytic activity toward a wide scope of feedstocks.

Results

Catalyst characterization. Binuclear zinc catalyst ($Zn_2L(NO_3)_2$, **1**) was prepared according to previously reported procedure with minor modification (Methods)[26,27]. Single-crystal X-ray diffraction (SCXRD) showed that $Zn_2L(NO_3)_2$ contains a μ_2-O bridged Zn–Zn with a distance of 3.2 Å (Extended Data Fig. 1a and Supplementary Table 3), close to that of binuclear metallohydrolases (3.5 ± 0.5 Å). X-ray absorption

near-edge structure (XANES) spectroscopy revealed that the Zn K-edge of **1** shifted to higher energy compared to that of Zn foil and ZnO (Fig. 2a), suggesting a higher oxidation state of zinc in **1** than the references. Fourier transforms of extended X-ray absorption fine structure (EXAFS) confirmed that the Zn atoms in **1** were coordinated to N/O atoms without Zn – Zn bond (Fig. 2b). These results indicate that the structure of **1** resembles the binuclear active site of OpdA (Fig. 1). We further loaded **1** on carbon support (Zn_2/C) for the convenience of catalyst separation and recycling. High-angle annular dark-field scanning transmission electron microscopy (HAADF-STEM) demonstrated the uniform distribution of **1** on the support (Fig. 2c). The XANES and the Fourier transforms of EXAFS spectra of the Zn_2/C were identical to that of **1** (Fig. 2a,b), manifesting that the catalyst structure remained after loading.

PET depolymerization under environmental conditions. The PET depolymerization kinetics was first evaluated under environmentally relevant conditions (pH 8 or seawater), using an amorphous PET (am-PET, from Goodfellow) as the substrate. In the presence of the Zn_2/C, the am-PET was completely depolymerized into monomers within 10 weeks at pH 8 and 40 ^{o}C (Fig. 3a), with a specific activity of 36 $mg_{PET}\ d^{-1}\ g_{catal}^{-1}$ of terephthalate. For comparison, conventional hydrolysis catalysts, such as zinc acetate and zinc oxide were completely inactive at the same condition (Fig. 3a). This comparison suggests the unique activity of the Zn_2/C for breaking down the chemically inert PET under environmentally relevant condition.

To further evaluate the performance of Zn_2/C, we compared it with a commercially available PET-degrading enzyme, namely *Humicola insolens* cutinase (HiC). It should be noted that the commercial HiC is not the best-performing enzyme and we used it as the benchmark catalyst simply because it is widely available across labs. The comparison was conducted at pH 8 and 60 ^{o}C, an optimal condition for the commercial HiC. The commercial HiC showed a faster reaction rate at the beginning of the hydrolysis, but soon reached a plateau at a conversion of 40% (Fig. 3b). This plateau may result from different causes such as product inhibition or enzyme denaturation[28–30]. Most PET-degrading enzymes have limited capability to depolymerize high-crystalline PET (20%) that are commonly found in PET products[11,21,28], with no exception to the commercial HiC (Fig. 3b). In contrast, the hydrolysis kinetics of crystalline PET granule (38%) over Zn_2/C was in parallel to that of am-PET at pH 8 and 60 ^{o}C (Fig. 3b), indicating the crystallinity of PET feedstock has limited impact on the hydrolysis kinetics of Zn_2/C.

Given that oceans' average pH is around 8.1, the Zn_2/C is of great potential for plastic remediation in the marine environment. As a proof-of-concept demonstration, we investigated the depolymerization of crystalline PET granule (38%) in the seawater from the Yellow Sea of China (pH 7.9). In the presence of Zn_2/C, an ethylene glycol yield of 10% was observed in the seawater at 40 ^{o}C for 12 weeks (Fig. 3c). The control experiments showed that the PET granule (38%) is highly resistant to degradation without the binuclear catalyst or using zinc acetate as the catalyst. It is also worth noting that much-accelerated PET depolymerization under environmental conditions has not been recorded previously for abiotic catalysis.

In vitro studies have demonstrated that the catalytic efficiency of binuclear hydrolases has obvious correlation with the nature of metal ions[23,31]. It encouraged us to synthesize other binuclear derivatives using the same Robson-type ligand. The specific activities of the binuclear catalysts follow the order of di-Zn(II) > di-Cu(II) > di-Ni(II) > di-Co(II) > di-Fe(II) (Fig. 3d), at pH 8 and 60 ^{o}C. This order is in line with the Lewis acid strength of divalent metal ions. The greater Lewis acidity of Zn(II) could bind the carbonyl group in PET and activate it for nucleophilic attack, as revealed by the following mechanism study (Fig. 4).

Intramolecular reaction pathway. To understand the unusual activity of the catalyst, we followed the catalyst evolution throughout the PET hydrolysis at pH 8 and found that it took an intramolecular pathway to achieve the rate enhancement (Fig. 4a and Extended Data Fig. 2), exactly as OpdA and many other hydrolases do. We first noticed that the hydrolysis kinetics over the $Zn_2L(NO_3)_2$ (**1**) experienced an induction period during which the depolymerization proceeded at a quite slow rate (Fig. 3b and Fig. 4b). In many cases, induction period could be an indicator of pre-catalyst activation. Mass spectrometry (MS) was therefore performed to investigate the possible transformation of **1** during this period. It was revealed that **1** evolved to hydroxyl- or water-coordinated binuclear zinc species after 45 hours (Fig. 4b). Considering the latter was likely to be the active catalyst, we dissolved **1** in PET-free NaOH solution (0.1 M) and obtained a hydroxyl-coordinated binuclear Zn complex ($Zn_2L(OH)_2$, **2**, Extended Data Fig. 1b). Compared with **1**, the initial lag phase was significantly suppressed when **2** was subject to PET hydrolysis (Extended Data Fig. 3a). These results imply that **1** is a pre-catalyst and in-situ generated binuclear zinc hydroxide species participate in the catalytic cycle most likely.

We then investigated the adsorption of carbonyl group using diffuse reflection infrared Fourier transform spectroscopy (DRIFTS). With the presence of the binuclear zinc sites, the carbonyl stretch presented a red shift from 1719 cm^{-1} to 1704 cm^{-1} (Fig. 4c). It suggests a bond-weakening effect on the carbonyl group upon coordination to zinc, whereby the electrophilicity of the substrate is enhanced[32–34]. EXAFS evidenced that the coordination number (CN) of the zinc indeed increased during the reaction (Extended Data Fig. 4), which came with a geometry switch between in-plane and out-of-plane modes (Extended Data Fig. 5). Density functional theory (DFT) calculations, performed using ethylene glycol dibenzoate (EGD) as a model compound, also support that the binuclear catalyst can stably bind to hydroxyl and carbonyl group in EGD compound via two neighboring zinc sites. (**3**,**4**, Fig. 4a,d). The intermediate state (**3**) ties together the two reactants in a single molecule and transforms the hydrolysis into an intramolecular fashion. At this state, the ester carbonyl is primed for nucleophilic attack by the terminally bound hydroxyl in the immediate vicinity. The nucleophilic attack would lead to a cyclic intermediate (**4**, Fig. 4a). The μ_2-O bridged binuclear zinc sites are critical for the stabilization of **4** by forming a six-membered ring (Zn–O–C–O–Zn–μ_2-O). According to DFT, a configurational change of EGD was required to form the six-membered intermediate (**4**), and this process was the most endothermic step with energy cost of only 0.64 eV. Following **4**, the reaction proceeds via ester bond cleavage. The active center is temporally coordinated by the newly formed carboxylate (**5**, Fig. 4a,d) and then restored after a ligand replacement by free hydroxide. We obtained the single crystal of a carboxylate-coordinated binuclear zinc

polymer $[Zn_2L(BDC)]_n$ (BDC: 1,4-benzenedicarboxylate) when free hydroxide was depleted in the reaction solution (Extended Data Fig. 1c), providing circumstantial evidence of the last step. The calculated potential energy profiles indicate that the whole process is energetically feasible under the reaction conditions (Fig. 4d). In particular, DFT calculations also suggest that water molecules play essential roles in the catalytic process by stabilizing the under-coordinated Zn atom as well as strengthening Zn–O(EGD) binding, as detailed in Supplementary information. We conjectured that the coordination of water to the metal site could occur via proton jump from the surrounding water hydrogen-bonded to the hydroxyl group on the zinc, as implied by the SCXRD of $Zn_2L(OH)_2$ (**2**) (Extended Data Fig. 1d)[35,36].

PET recycling. In addition to accelerating PET degradation in the environment, the Zn_2/C also provides a solution to scalable PET recycling. We first evaluated the catalytic activities of Zn_2/C over a wide range of operational conditions (30–90 ^oC, pH 8–14). The Zn_2/C functioned normally under all conditions and its specific activity increased significantly with the rises of temperature and pH (Extended Data Fig. 3b). Further stability test indicated that the binuclear catalyst maintained stable below 340 ^oC (Extended Data Fig. 3c). We then performed the PET recycling at pH 13 and 90 ^oC to have a trade-off between productivity and energy-efficiency. The Zn_2/C delivered a specific activity of 577 ± 35 $g_{PET}\ h^{-1}\ g_{catal}^{-1}$ (Methods, Fig. 5a, Extended Data Fig. 3d), outperforming the other recycling processes, even though it was performed under relatively lower temperature and/or weaker alkaline condition (Supplementary Table 1). As compared in Supplementary Table 1, the glycolysis (e.g., the Volcat process) is typically performed at temperatures above 160 ^oC in the presence of organic bases such as 1,5,7-triazabicyclo[4.4.0]dec-5-ene (TBD) and 1,8-diazabicyclo[5.4.0]undec-7-ene (DBU), while the alkaline hydrolysis is usually carried out at 80–150 ^oC in 1–5 M alkaline solutions. The Zn_2/C had an industrially feasible space-time yield of 50–70 $g\ L^{-1}\ h^{-1}$ of terephthalate, depending on catalyst loadings (Fig. 5a, Supplementary Table 1). Catalyst reusability is another important measure for industrial practice. The Zn_2/C exhibited a yield decrease of about 8% after 15 cycles of reuse, with a turnover number (TON) > 25000 realized (Fig. 5b). The percentage of zinc loss per cycle was investigated using inductively coupled plasma optical emission spectroscopy (ICP-OES) (Fig. 5b). There was 4.6% of zinc was lost in the first cycle and then the number dropped below 1% in the subsequent cycles. The structure of the spent Zn_2/C remained the same as its original form according to electron microscopy and X-ray absorption spectroscopy (Extended Data Fig. 6).

To make a step toward real-world applications, we submitted the binuclear catalyst to different PET feedstocks. The post-consumer PET waste is of high crystallinity and complex mixtures. The specific activities of the Zn_2/C toward different crystalline PET waste reached 65–82% of the activity for am-PET (2.9 $mg\ h^{-1}\ mg_{catal}^{-1}$ at pH 13 and 60 ^oC) (Methods, Fig. 5c, Extended Data Fig. 7). The impurities and additives in these post-consumer PET products, i.e. dyed bottle, cloth fiber, and carpet, didn't compromise the catalyst performance obviously, as their activities were on a par with the additive-free granule. In addition to the crystallinity issue, plastic waste is usually composed of mixed polymers. This complexity in the waste streams bears another technological challenge[9,37]. The Zn_2/C presented very consistent

performance toward the physical mixtures of PET with a variety of plastics (Fig. 5c), including polystyrene (PS), polyvinylchloride (PVC), polylactic acid (PLA), polycaprolactone (PCL), polypropylene (PP), and polyethylene (PE). These results suggest that the Zn_2/C is competent to cope with real-life PET waste.

To demonstrate a closed-loop PET recycling (Methods, Extended Data Fig. 8a,b), post-consumer PET waste was processed in a 5 liter reactor at pH 13 and 90 ^{o}C, with a PET/catalyst ratio of 500 $g_{PET}\ g_{catal}^{-1}$ and a solids content of 16.7 wt%. The purity of the recovered terephthalic acid was above 99% as confirmed by ^{1}H nuclear magnetic resonance (NMR) and high-performance liquid chromatography (Extended Data Fig. 8c,d). The recovered monomer (terephthalic acid) was then used as raw material to make recycled PET (rPET). The characteristics of the rPET were similar to those of PET made from virgin pure terephthalic acid (Extended Data Fig. 8e), meeting the standard of bottle-grade PET. A tentative technoeconomic assessment indicated that the above process could generate a net profit of 26.0 million USD on 0.1 megatons of PET waste per year (Extended Data Fig. 9 and Supplementary Information).

The synthetic binuclear catalyst features an open-access active site, which can depolymerize a wide spectrum of substrates. This is particularly important for environmental remediation, as there are different types of plastic waste to remove from soil or water. We demonstrated that the Zn_2/C was catalytically active for 13 different kinds of polyesters and Nylon 66 (Fig. 5c and Extended Data Fig. 10). Highlights include polylactic acid (PLA) (9.1 $mg_{monomer}\ h^{-1}\ mg_{catal}^{-1}$), polybutylene adipate terephthalate (PBAT) (3.0 $mg_{monomer}\ h^{-1}\ mg_{catal}^{-1}$), polycaprolactone (PCL) (9.4 $mg_{monomer}\ h^{-1}\ mg_{catal}^{-1}$), and PU (12.2 $mg_{monomer}\ h^{-1}\ mg_{catal}^{-1}$). Asides from polyesters, considerable degradation of Nylon 66 was also observed over this catalyst at pH 13 and 60 ^{o}C, with a specific activity of 0.11 $mg_{monomer}\ h^{-1}\ mg_{catal}^{-1}$. The capacity of Zn_2/C to digest recalcitrant polyamide (Nylon 66) warrants further attention, as few enzymes can do. It should be mentioned that the substrate universality does not compromise centralized PET recycling, because the collection and sorting of PET waste is already involved in current recycling industry.

Discussion

In summary, we designed a binuclear zinc catalyst for polyester depolymerization. The biomimetic Zn–Zn sites endow the hydrolysis with an intramolecular character by binding plastic substrate and nucleophile together. This proximity effect can bring enormous rate enhancement under environmental conditions (pH 8 and 40 ^{o}C), as manifested by considerable PET depolymerization in the seawater in 12 weeks (36 $mg_{PET}\ d^{-1}\ g_{catal}^{-1}$). This character can also generate energy savings to PET recycling under much less-demanding conditions (pH 13 and 90 ^{o}C) compared to conventional chemical recycling (Supplementary Table 1), delivering a specific activity of as high as 577 $g_{PET}\ h^{-1}\ g_{catal}^{-1}$. We also showcased closed-loop manufacturing of recycled PET (rPET) of virgin quality. We further demonstrated the compatibility of this binuclear catalyst with complex mixtures in plastic waste and its wide substrate

scope. Considering the structure of the reported binuclear zinc complex can be further tailored in many ways, we anticipate this work will serve as a starting point for more efficient plastic-degrading catalysts to be developed.

Methods

Syntheses of the catalysts. Binuclear complexes [$Zn_2C_{25}H_{28}N_6O_9$, $Zn_2L(NO_3)_2$] was prepared according to procedures previously reported with minor modifications[26,27]. The obtained compounds were characterized by elemental analysis, infrared spectroscopy, powder X-ray diffraction (PXRD), and single-crystal X-ray diffraction (SCXRD), respectively. Single crystals of the reaction intermediates [$Zn_2C_{24}H_{44}N_4O_{12}$, $Zn_2L(OH)_2$] and {$Zn_2C_{32}H_{30}N_4O_6$, $[Zn_2L(BDC)]_n$} obtained from the reaction solution were directly subjected to SCXRD without further treatment.

$Zn_2L(NO_3)_2$: In a typical synthesis of $Zn_2L(NO_3)_2$ (**1**), $Zn(NO_3)_2{\cdot}6H_2O$ (0.446 g, 1.5 mmol) was dissolved in methanol (5 mL) in a round-bottom flask (25 mL). Methanol solutions of 1,3-diaminopropane (0.111 g, 0.75 M, 2 mL) and 2-hydroxy-5-methylisophthalaldehyde (0.246 g, 0.2 M, 7.5 mL) were added into the flask to form a clear solution. After standing for two days at room temperature, yellow tabular crystals were collected and used directly for SCXRD. ^{1}H NMR (400 MHz, D_2O): δ 8.26 (s, 4H, N = CH), 7.34 (s, 4H, Ar), 3.92 (s, 8H, N–CH_2), 2.20 (s, 6H, Ar–CH_3), 2.04 (s, 4H, CH_2). Anal. Calcd (%) for $Zn_2C_{25}H_{28}N_6O_9$: C, 43.69; H, 4.11; N, 12.23. Found: C, 43.42; H, 4.21; N, 12.31. The crystal data was shown in Supplementary Table 2,3.

$Zn_2L(OH)_2$: Single crystals of $Zn_2L(OH)_2$ (**2**) were obtained *via* recrystallization from an aqueous solution of $Zn_2L(NO_3)_2$ and NaOH (0.1 M). The crystals exhibited high quality and were suitable for SCXRD. Additionally, $Zn_2L(OH)_2$ crystals were also obtained from the reaction mixture during PET hydrolysis at pH 13 and confirmed by SCXRD and PXRD. Anal. Calcd (%) for $Zn_2C_{24}H_{44}N_4O_{12}$: C, 40.52; H, 6.23; N, 7.88. Found: C, 40.47; H, 6.21; N, 7.81. The crystal data was shown in Supplementary Table 2,4.

$[Zn_2L(BDC)]_n$: Coordination polymer $[Zn_2L(BDC)]_n$ (BDC refers to 1,4-benzenedicarboxylate) was obtained as a hydrolysis intermediate from the reaction mixture when hydroxide ions were depleted during PET depolymerization. Specifically, $Zn_2L(OH)_2$ (7.1 mg, 10 μmol) and PET (1.9 mg) were added into 10 mL deionized water and heated at 90°C for 12 h without stirring. After cooling to room temperature, yellow prism crystals were collected. Anal. Calcd (%) for $Zn_2C_{32}H_{30}N_4O_6$: C, 55.11; H, 4.34; N, 8.03. Found: C, 55.17; H, 4.21; N, 7.91. The crystal data was shown in Supplementary Table 2,5.

Zn_2/C: High-surface area carbon support (Ketjenblack EC-300J, 20 mg) was dispersed in 20 mL of methanol/water mixture ($V_{methanol}$: V_{water} = 1:1). The dispersion was ultrasonicated for 10 min. In the meantime, 4 mg of $Zn_2L(NO_3)_2$ was dissolved in 10 mL of methanol/water mixture ($V_{methanol}$: V_{water} = 1:1). Subsequently, the solution of $Zn_2L(NO_3)_2$ was added into the carbon dispersion and the mixture was ultrasonicated for another 10 minutes. Finally, the solid product was collected by filtration and dried in

vacuum oven. The content of metal Zn is 3.1 wt% based on inductively coupled plasma optical emission spectrometer (ICP-OES) and elemental analysis.

Preparation of polyester powders. Amorphous PET film (Goodfellow Ltd, ES301445) was pretreated by liquid nitrogen and then micronized into powders with diameters of 100 to 500 μm. Crystalline PET granule (Macklin, P875573, crystallinity of 38%) was micronized into powders with diameters of 100 to 500 μm. Post-consumer PET water bottles (Nongfu spring, China) and PET dyed beverage bottles (Danone, France; Coca-Cola, USA, crystallinity of 25%) were collected from a local recycling site and were cut into 10 × 10 mm pieces before depolymerization. Cloth fibers and pink carpet were purchased online labeling 100% PET and were cut into 10 × 10 mm pieces before depolymerization. PCL granule (Energy Chemical, A022136, M_W~50000, diameters of 3 mm, crystallinity of 20%), PBAT granule (Macklin, P909229, M_n~120000, diameters of 3 mm, crystallinity of 30%), PLA granule (Macklin, P909229, M_n~80000, diameters of 3 mm, crystallinity of 25%), PA granule (HEOWNS, N99410, Nylon66, diameters of 0.2 mm, crystallinity of 40%), PGA granule (Yuanye Bio-Technology, S28547, M_n~100000, diameters of 3 mm, crystallinity of 50%), PBA granule (Macklin, P916125, M_W~2000, diameters of 3 mm, crystallinity of 25%), PBS granule (HEOWNS, P68985, diameters of 3 mm, crystallinity of 50%), PC granule (Macklin, P888352, M_W~26000, diameters of 3 mm, crystallinity of 10%), and PBT granule (Macklin, P909269, diameters of 3 mm, crystallinity of 30%) were not pretreated before use. PU, PEF, PHB and P3/4HB were purchased online with diameters of 0.5 mm and crystallinity of 30%.

PET hydrolysis under environmentally relevant condition. PET hydrolysis was performed in a 20 mL vial placed in an aluminum heating block on a stirring hotplate. The vial was charged with a magnetic stirring bar, 10 mg of PET, and zinc-containing catalysts (0.8 mg in terms of zinc). 10 mL of NaOH solution (pH 8) or natural seawater (Yellow Sea, China, pH 7.9) was then added into the mixture under stirring. The stirring speed was kept at 400 rpm throughout the reaction, whereby the external mass transfer limitations were eliminated. The reaction solution was heated to designed temperatures to initiate the hydrolysis, and aliquots were taken and analyzed by ^{1}H NMR. The hydrolysis of PET yielded the same molar amount of disodium terephthalate and ethylene glycol. Due to the low solubility of disodium terephthalate at pH 8, the ^{1}H NMR of ethylene glycol was used to calculate the conversion of PET using maleic acid as the internal standard. The pH of the reaction solution was maintained constant during the reaction by adding NaOH. For PET hydrolysis over HiC (0.48 g, Novozym 51032, 6 wt%), the hydrolysis was conducted in the same way except that potassium phosphate buffer (pH 8, 1.0 M) was used instead of NaOH solution.

PET hydrolysis under industrially relevant condition

PET hydrolysis was optimized at pH 13 and 90 ^{o}C in a 250 mL three-necked flask. The flask was charged with a mechanical stirrer, 50 g of PET, and 5–50 mg $Zn_2L(NO_3)_2$ supported on carbon. 50 mL of NaOH solution (pH 13) was then added into the mixture under stirring. The stirring speed was kept at 300 rpm throughout the reaction. The reaction solution was heated to 90 ^{o}C. The kinetics of the PET

depolymerization was determined by using base consumption (Extended Data Fig. 3d). The pH value was maintained constant at 13 during the reaction by adding NaOH.

Post-consumer PET waste recycling

Post-consumer PET waste was collected from dumpsters around campus and shredded into ca. 10 mm by 10 mm pieces. Then, we added these pieces into a 5 L flask with Zn_2/C and adjusted the pH to 13 using NaOH. The reaction mixture was heated up to 90°C while periodically adding sodium hydroxide to maintain its pH at around 13. After the reaction, Zn_2/C was recycled by vacuum filtration using a Buchner funnel. The solid Zn_2/C was collected on the top of a filter paper to form a black filter cake for reuse. Thereafter, acidification process was performed by adding sulfuric acid to convert soluble disodium terephthalate into terephthalic acid precipitation. After washing with deionized water twice and drying in oven overnight, pure terephthalic acid (PTA) was gained. ^{1}H NMR and High-Performance Liquid Chromatography (HPLC) were performed to test the purity of the product (Extended Data Fig. 8). The purity of the recycled PTA was above 99% according to the national standard GB/T 30921.1. The content of 4-hydroxybenzaldehyde impurity was 8 mg kg^{-1}, less than that of virgin PTA (11 mg kg^{-1}). The recycled PTA was then used to synthesize PET.

Hydrolysis of different polymeric substrates. Substrate screening was performed in a 20 mL vial placed in an aluminum heating block on a stirring hotplate. The vial was charged with a magnetic stirring bar, 0.32 g of different PET feedstocks, polyesters or polyamide, and 2 mg $Zn_2L(NO_3)_2$ supported on carbon. 10 mL of NaOH solution (pH 13) was then added into the mixture under stirring. The stirring speed was kept at 400 rpm throughout the reaction. The reaction solution was heated to 60°C to initiate the hydrolysis, and aliquots were taken and analyzed by the ^{1}H NMR of the corresponding monomers generated during hydrolysis of different polymeric substrates. The pH was maintained constant during the reaction by adding NaOH.

DFT calculations. Spin-polarized DFT calculations were performed with the projector-augmented-wave (PAW) method[38,39] and the Perdew – Burke – Ernzerhof (PBE) exchange-correlation functional[40] as implemented in the *Vienna Ab Initio Simulation Package* (VASP)[38,41]. The kinetic energy cutoff of 400 eV was employed. Gaussian smearing with a width of 0.05 eV was used. The total energy was converged better than 10^{-4} eV/atom, and the final force on each atom was less than 0.05 eV/Å. The first Brillouin zone was sampled on a Γ point. The van der Waals (vdW) corrections were calculated with DFT-D2 method of Grimme to describe precise energies with dispersions. To capture the intermediates, the cluster model was constructed within a vacuum cubic of 20 × 20 × 20 Å. In the calculation of potential energy profile references, the DFT energies of gaseous H_2O and hydroxyl (OH^-) were calibrated to liquid water and solvated hydroxyl ion (OH^-) in aqueous at room temperature according to the standard reference[42].

More details on DFT calculations are provided in Supplementary Information.

Abbreviations	Synonyms	Formulas
PET	Polyester terephthalate	
EGD	Ethylene glycol dibenzoate	$C_{16}H_{14}O_4$
EGM	Ethylene glycol monobenzoate	$C_9H_{10}O_3$
BzA	Benzoic acid	$C_8H_5O_2$
BzO	Benzoate	$[C_7H_5O_2]^-$
$Zn_2L(OH)_2$ (cluster)		$Zn_2C_{24}H_{26}N_4O_4$

Characterization. Single-crystal X-ray diffraction (SCXRD) data were collected at 173 K on a SuperNova charge-coupled device (CCD) X-ray diffractometer, with Cu-Kα radiation (λ = 1.54184 Å). Powder X-ray diffraction (XRD) patterns were recorded on a Rigaku D/MAX-2500 diffractometer using a filtered Cu-Kα radiation source (λ = 1.54056 Å). High angle angular dark field-scanning transmission electron microscopy (HADDF-STEM) image was acquired by a JEM-ARM200F transmission electron microscope operated at 200 keV, equipped with a probe spherical aberration corrector. Matrix assisted laser desorption ionization-time of flight mass (MALDI-TOF MS) was carried out with AXIMA-Performance (Shimadzu). Differential scanning calorimetry (DSC) measurements were performed with Q200 of TA Instrument. DRIFTS was obtained via a Fourier transform infrared spectrometer (Thermo Nicolet iS50) equipped with a diffuse reflection accessory (Harrick Inc.). ^{1}H NMR was recorded by AVANCE (Bruker). The XAFS spectra at Zn K-edge were acquired at the 4B9A station in Beijing Synchrotron Radiation Facility (BSRF), operated at 2.5 GeV with a maximum current of 250 mA.

Declarations

Data availability

The data that support the findings of this study are available within the article and Supplementary Information. Source data are available from the corresponding author upon reasonable request. Crystallographic data for the structures reported in this Article have been deposited at the Cambridge Crystallographic Data Centre, under deposition nos. CCDC 2082457 (**$Zn_2L(NO_3)$**), 2082456 (**$Zn_2L(OH)_2$**) and 2113556 (**$[Zn_2L(BDC)]_n$**). Copies of the data can be obtained free of charge via https://www.ccdc.cam.ac.uk/structures/.

Acknowledgements

This work was supported by the National Key R&D Program of China (2019YFA0709200), the National Natural Science Foundation of China (22075162), and China Postdoctoral Science Foundation (2021M691754). The DFT calculations were performed using computational resources at the Center for

Functional Nanomaterials, a user facility at Brookhaven National Laboratory supported by the U.S. DOE under Contract DE-SC0012704. We acknowledge the BL14W1 station in Shanghai Synchrotron Radiation Facility (SSRF) and 4B9A station in Beijing Synchrotron Radiation Facility (BSRF) for the collection of XAFS data.

Author Contributions

Z.N. conceptualized and guided this work. Z.N. and S.Z. designed the experiments. S.Z., Q.H. and Y.-X.Z. performed the experiments and contributed equally to this work. H.G., and P.L. performed the DFT calculations. X.Z. carried out the production and characterization of rPET using recycled PTA. Z.N., S.Z., Q.H., Y.-X.Z., H.G. and P.L. wrote the paper. All the authors participated in the data analysis and commented on the manuscript.

Competing interests

Z.N., S.Z., Q.H. and Y.-X.Z. have filed a PCT patent. X.Z. is the employee of Sinopec Yizheng Chemical Fibre Co., Ltd.

References

1. Rochman, C. M., Browne, M. A., Halpern, B. S., Hentschel, B. T., Hoh, E., Karapanagioti, H. K., Rios-Mendoza, L. M., Takada, H., Teh, S., & Thompson, R. C. Policy: classify plastic waste as hazardous. Nature **494**, 169–171 (2013).
2. Guha Roy, A. Detailing plastic pollution. Nat. Sustain. **2**, 654 (2019).
3. Geyer, R. J., Jambeck, R., & Law, K. L. Production, use, and fate of all plastics ever made. Sci. Adv. **3**, e1700782 (2017).
4. MacLeod, M., Arp, H. P. H., Tekman, M. B., & Jahnke, A. The global threat from plastic pollution. Science **373**, 61–65 (2021).
5. Zhang, Z., Gora-Marek, K., Watson, J. S., Tian, J., Ryder, M. R., Tarach, K. A., López-Pérez, L., Martínez-Triguero, J., & Melián-Cabrera, I. Recovering waste plastics using shape-selective nano-scale reactors as catalysts. Nat. Sustain. **2**, 39–42 (2019).
6. Jambeck, J. R., Geyer, R., Wilcox, C., Siegler, T. R., Perryman, M., Andrady, A., Narayan, R., & Law, K. L. Plastic waste inputs from land into the ocean. Science **347**, 768–771 (2015).
7. George, N. & Kurian, T. Recent developments in the chemical recycling of postconsumer poly(ethylene terephthalate) waste. Ind. Eng. Chem. Res. **53**, 14185–14198 (2014).
8. Chen, C-C., Han, X., Li, X., Jiang, P., Niu, D., Ma, L., Liu, W., Li, S., Qu, Y., Hu, H., Min, J., Yang, Y., Zhang, L., Zeng, W., Huang, J-W., Dai, L., & R-T. Guo, General features to enhance enzymatic activity of poly(ethylene terephthalate) hydrolysis. Nat. Catal. **4**, 425–430 (2021).
9. Ellis, L. D., Rorrer, N. A., Sullivan, K. P., Otto, M., McGeehan, J. E., Román-Leshkov, Y., Wierckx, N., & Beckham, G. T. Chemical and biological catalysis for plastics recycling and upcycling. Nat. Catal. **4**,

539–556 (2021).

10. Zhu, B., Wang, D., & Wei, N. Enzyme discovery and engineering for sustainable plastic recycling. Trends in Biotechnology, **40**, 22–37 (2022).
11. Tournier, V., Topham, C. M., Gilles, A., David, B., Folgoas, C., Moya-Leclair, E., Kamionka, E., Desrousseaux, M.-L., Texier, H., Gavalda, S., Cot, M., Guémard, E., Dalibey, M., Nomme, J., Cioci, G., Barbe, S., Chateau, M., André, I., Duquesne, S., & Marty, A. An engineered PET depolymerase to break down and recycle plastic bottles. Nature **580**, 216–219 (2020).
12. Tokiwa, Y. & Suzuki, T. Hydrolysis of polyesters by lipases. Nature **270**, 76–78 (1977).
13. DelRe, C., Jiang, Y., Kang, P., Kwon, J., Hall, A., Jayapurna, I., Ruan, Z., Ma, L., Zolkin, K., Li, T., Scown, C. D., Ritchie, R. O., Russell, T. P., & Xu, T. Near-complete depolymerization of polyesters with nano-dispersed enzymes. Nature **592**, 558–563 (2021).
14. Samak, N. A., Jia, Y., Sharshar, M. M., Mu, T., Yang, M., Peh, S., & Xing, J. Recent advances in biocatalysts engineering for polyethylene terephthalate plastic waste green recycling. Environ. Int., **145**, 106144 (2020).
15. Yoshida, S., Hiraga, K., Takehana, T., Taniguchi, I., Yamaji, H., Maeda, Y., Toyohara, K., Miyamoto, K., Kimura, Y., & Oda, K. A bacterium that degrades and assimilates poly(ethylene terephthalate). Science **351**, 1196–1199 (2016).
16. Štrukil, V. Highly efficient solid-state hydrolysis of waste polyethylene terephthalate by mechanochemical milling and vapor-assisted aging. ChemSusChem, **14**, 330–338 (2021).
17. Han, X., Liu, W., Huang, J-W., Ma, J., Zheng, Y., Ko, T-P., Xu, L., Cheng, Y-S., Chen, C-C., & Guo, R-T. Structural insight into catalytic mechanism of PET hydrolase. Nat. Commun. **8**, 2106 (2017).
18. Joo, S., Cho, I. J., Seo, H., Son, H. F., Sagong, H-Y., Shin, T. J., Choi, S. Y., Lee, S. Y., & Kim, K-J. Structural insight into molecular mechanism of poly(ethyleneterephthalate) degradation. Nat. Commun. **9**, 382 (2018).
19. Austin, H. P., Allen, M. D., Donohoe, B. S., Rorrer, N. A., Kearns, F. L., Silveira, R. L., Pollard, B. C., Dominick, G., Duman, R., Omari, K. E., Mykhaylyk, V., Wagner, A., Michener, W. E., Amore, A., Skaf, M. S., Crowley, M. F., Thorne, A. W., Johnson, C. W., Woodcock, H. L., McGeehan, J. E., & Beckham, G. T. Characterization and engineering of a plastic-degrading aromatic polyesterase. *Proc. Natl Acad. Sci. USA*, **115**, E4350–E4357 (2018).
20. Pinto, A. V., Ferreira, P., Neves, R. P., Fernandes, P. A., Ramos, M. J., & Magalhaes, A. L. Reaction mechanism of MHETase, a PET degrading enzyme. ACS Catal. **11**, 10416–10428 (2021).
21. Kawai, F., Kawabata, T. & Oda, M. Current knowledge on enzymatic PET degradation and its possible application to waste stream management and other fields. Appl. Microbiol. Biotechnol. **103**, 4253–4268 (2019).
22. Schwizer, F., Okamoto, Y., Heinisch, T., Gu, Y., Pellizzoni, M. M., Lebrun, V., Reuter, R., Köhler, V., Lewis, J. C., & Ward, T. R. Artificial metalloenzymes: reaction scope and optimization strategies. Chem. Rev. **118**, 142–231(2018).

23. Schenk, G., Mitic, N., Gahan, L. R., Ollis, D. L., McGeary, R. P., & Guddat, L. W. Binuclear metallohydrolases: complex mechanistic strategies for a simple chemical reaction. Acc. Chem. Res. **45**, 1593–1603 (2012).
24. Wilcox, D. E. Binuclear metallohydrolases. Chem. Rev. **96**, 2435–2458 (1996).
25. Hadler, K. S., Tanifum, E. A., Yip, S. H-C., Mitić, N., Guddat, L. W., Jackson, C. J., Gahan, L. R., Nguyen, K., Carr, P. D., Ollis, D. L., Hengge, A. C., Larrabee, J. A., & Schenk, G. Substrate-promoted formation of a catalytically competent binuclear center and regulation of reactivity in a glycerophosphodiesterase from Enterobacter aerogenes. J. Am. Chem. Soc. **130**, 14129–14138 (2008).
26. Pilkinqton, N. H., & Robson, R. Complexes of binucleating ligands III. Novel conplexes of a macrocyclic Binucleating ligand. Aust. J. Chem., **23**, 2225–2236 (1970).
27. Dutta, B., Bag, P., Flo1rke, U., & Nag, K. Dinuclear Zn(II) complexes of tetraiminodiphenol macrocycles and their interactions with carboxylate anions and amino acids. photoluminescence, equilibria, and structure. Inorg. Chem. **44**, 147–157 (2005).
28. Kaabel, S., Therien, J. D., Deschênes, C. E., Duncan, D., Friščić, T., & Auclair, K. Enzymatic depolymerization of highly crystalline polyethylene terephthalate enabled in moist-solid reaction mixtures. *Proc. Natl Acad. Sci. USA* **118**, e2026452118 (2021).
29. Barth, M., Oeser, T., Wei, R., Then, J., Schmidt, J., & Zimmermann, W. Effect of hydrolysis products on the enzymatic degradation of polyethylene terephthalate nanoparticles by a polyester hydrolase from Thermobifida fusca. Biochem. Eng. J. **93**, 222–228(2015).
30. Singh, A., Rorrer, N. A., Nicholson, S. R., Erickson, E., DesVeaux, J. S., Avelino, A. F. T., Lamers, P., Bhatt, A., Zhang, Y., Avery, G., Tao, L., Pickford, A. R., Carpenter, A. C., McGeehan, J. E., & Beckham, G. T. Techno-economic, life-cycle, and socioeconomic impact analysis of enzymatic recycling of poly (ethylene terephthalate). Joule, **5**, 2479–2503 (2021).
31. Mitić, N., Smith, S. J., Neves, A., Guddat, L. W., Gahan, L. R., & Schenk, G. The catalytic mechanisms of binuclear metallohydrolases. Chem. Rev. **106**, 3338–3363 (2006).
32. Meng, X., Wang, L., Chen, L., Xu, M., Liu, N., Zhang, J., Yang, Y., & Wei, M. Charge-separated metal-couple-site in NiZn alloy catalysts towards furfural hydrodeoxygenation reaction. J. Catal. **392**, 69–79 (2020).
33. Wang, Y., Zhang, Y., Song, H., Wang, Y., Deng, T., & Hou, X. Zn-catalyzed ester bond cleavage: Chemical degradation of polyethylene terephthalate. J. Clean. Prod. **208**, 1469–1475 (2019).
34. Sammon, C., Yarwood, J., & Everall, N. An FT–IR study of the effect of hydrolytic degradation on the structure of thin PET films. Polym. Degrad. Stabil. **67**, 149–158 (2000).
35. Aziz, E. F., Ottosson, N., Faubel, M., Hertel, I. V., & Winter, B. Interaction between liquid water and hydroxide revealed by core-hole de-excitation. Nature, **455**, 89–91(2008).
36. Wolke, C. T., Fournier, J. A., Dzugan, L. C., Fagiani, M. R., Odbadrakh, T. T., Knorke, H., Jordan, K. D., McCoy, A. B., Asmis, K. R., & Johnson, M. A. Spectroscopic snapshots of the proton-transfer mechanism in water. Science, **354**, 1131–1135 (2016).

37. Westhues, S., Idel, J., & Klankermayer, J. Molecular catalyst systems as key enablers for tailored polyesters and polycarbonate recycling concepts. Sci. Adv. **4**, eaat9669 (2018).
38. Kresse, G., & Joubert, D. From ultrasoft pseudopotentials to the projector augmented-wave method. Phys. Rev. B **59**, 1758–1775 (1999).
39. Blöchl, P. E. Projector augmented-wave method. Phys. Rev. B **50**, 17953–17979 (1994).
40. Perdew, J. P., Burke, K., & Ernzerhof, M. Generalized gradient approximation made simple. Phys. Rev. Lett. **77**, 3865–3868 (1996).
41. Kresse, G., & Furthmüller, J. Efficient iterative schemes for Ab initio total-energy calculations using a plane-wave basis set. Phys. Rev. B **54**, 11169–11186 (1996).
42. Ebbing, D., & Gammon, S. D. *General Chem*. Cengage Learning (2016).

Figures

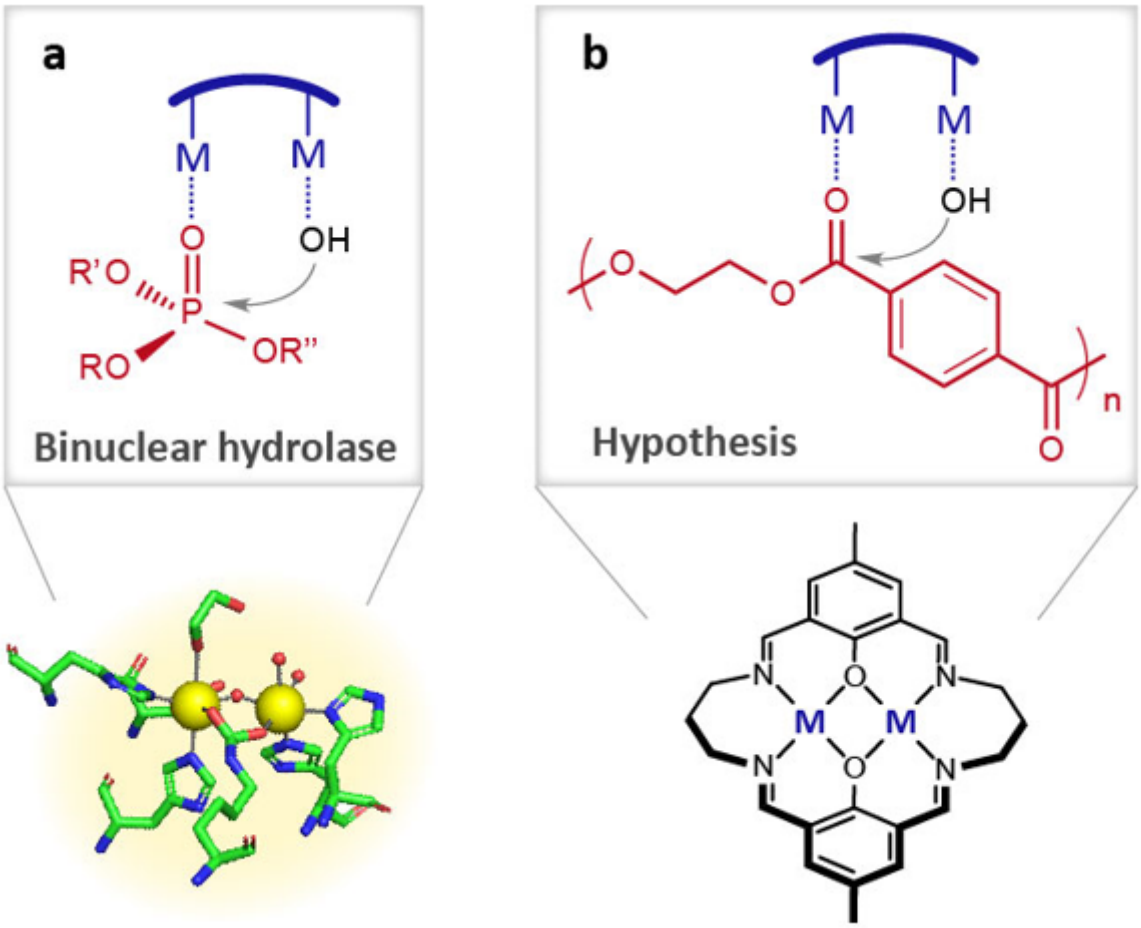

Figure 1

Binuclear catalyst design. Schematic representations of the active sites and reaction mechanisms proposed for binuclear hydrolase OpdA (**a**) and the hypothesized PET-degrading binuclear catalyst (**b**), where M represents metal sites, blue arcs represent active-site backbones. Note that the binuclear metal

centers in the hydrolase play critical roles in accelerating ester hydrolysis via the organization of substrates in close proximity, the electrophilic activation of esters, and the stabilization of transition states.

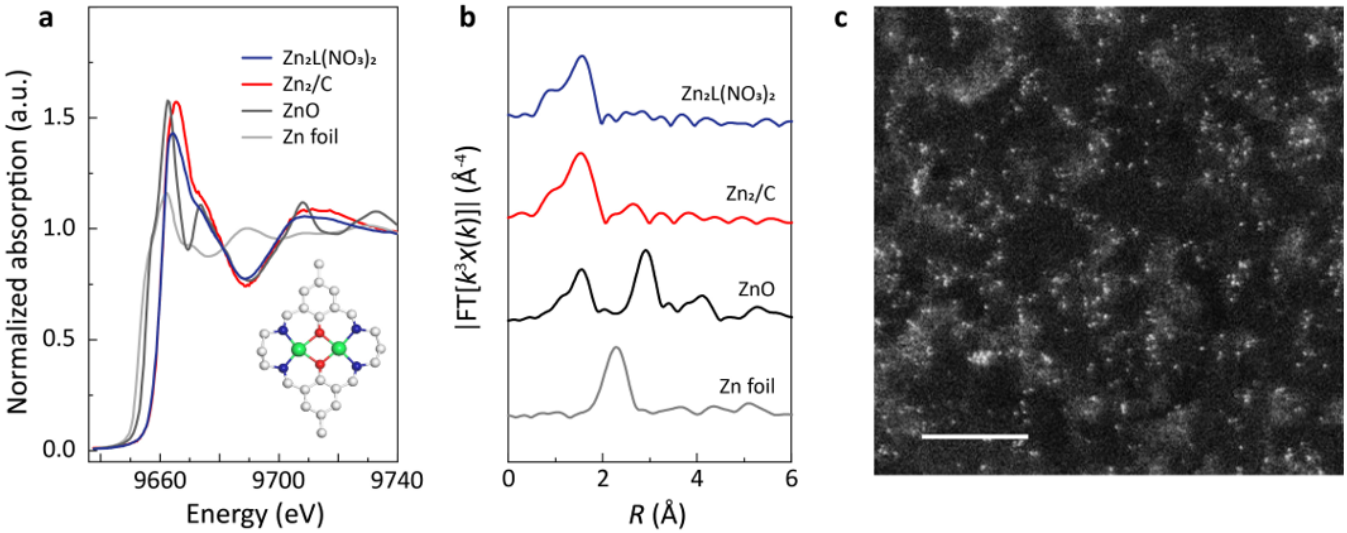

Figure 2

Structure characterizations of the binuclear catalyst. a, Normalized XANES spectra of $Zn_2L(NO_3)_2$, Zn_2/C, and references. The inset depicts the structure of Zn_2L, where the white, blue, red, and green balls represent C, N, O, Zn atoms, respectively. **b**, Fourier transforms of EXAFS spectra of $Zn_2L(NO_3)_2$, Zn_2/C, and references. **c**, The aberration-corrected HAADF-STEM of Zn_2/C (scale bar: 5 nm).

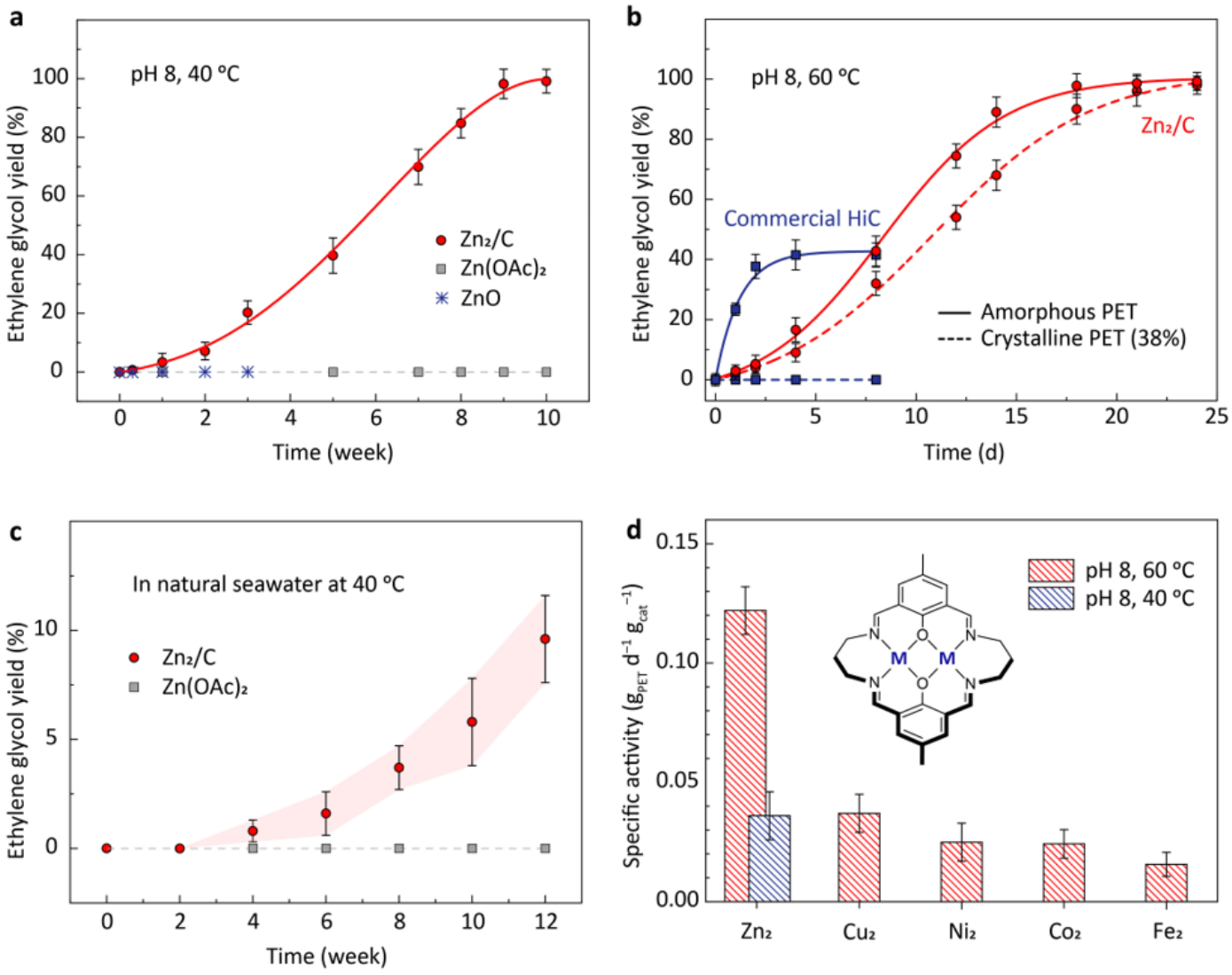

Figure 3

PET depolymerization under environmentally relevant conditions. a, The hydrolysis kinetics of am-PET over Zn_2/C, zinc acetate, and zinc oxide at pH 8 and 40 °C. **b**, The hydrolysis kinetics of am-PET and crystalline PET granule (38%) over Zn_2/C and commercial HiC at pH 8 (NaOH aqueous solution) and 60 °C, an optimal condition for the commercial HiC. Note that an induction period was observed over the binuclear catalyst. **c**, The hydrolysis kinetics of crystalline PET granule (38%) over Zn_2/C and zinc acetate in natural seawater (Yellow Sea, China, pH 7.9) at 40 °C (Methods). **d**, The specific activities of binuclear catalysts with different metal centers toward hydrolysis of crystalline PET granule (38%) at pH 8 (NaOH aqueous solution) and 60 °C. The specific activities were calculated at 18 days in 10 mL of NaOH aqueous solution containing 10 mg of PET and 4 mg of $Zn_2L(NO_3)_2$ supported on carbon. All the error bars in this figure represent the standard deviations for three measurements.

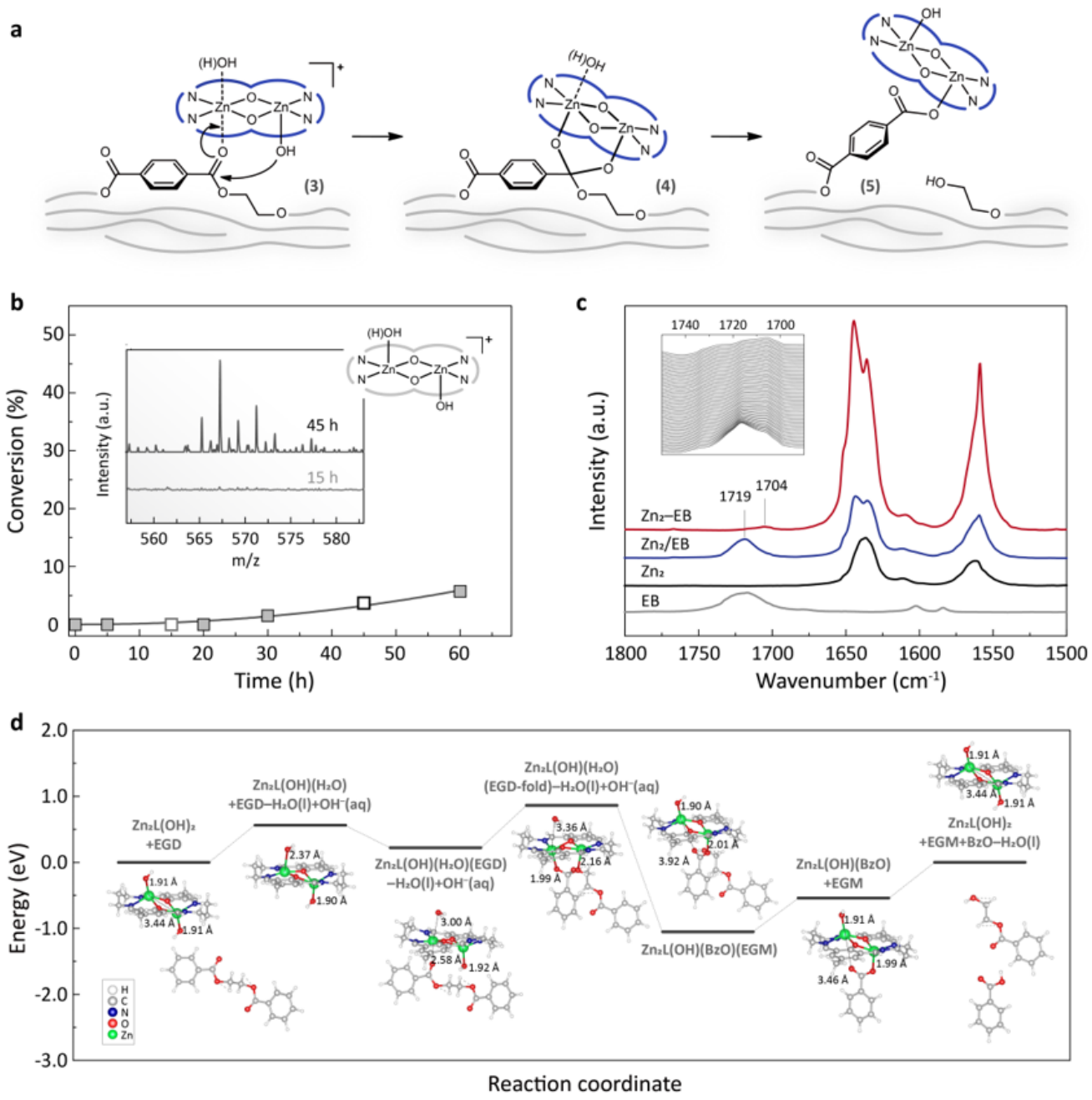

Figure 4

PET depolymerization mechanism over the binuclear catalyst. a, The key steps accounted for the PET hydrolysis over the binuclear catalyst, including the co-adsorption of substrates in the adjacent zinc sites (**3**) and the stabilization of six-membered intermediate (**4**). The blue loops represent the ligand backbones, and the grey lines represent the polymer chains. **b**, Induction period enlarged from the hydrolysis kinetics in Fig. 2d and the corresponding MS spectra at 15 and 45 h (inset). **c**, DRIFTS spectra of ethyl benzoate (EB), an analogue to PET but with low boiling point, over the binuclear zinc catalyst (Zn_2). The blue curve represents the physical mixture of Zn_2 and EB (Zn_2/EB) and the red curve shows the adsorption of EB on Zn_2 (Zn_2-EB). The inset depicts the DRIFT evolution from Zn_2/EB to Zn_2-EB during the removal of free and loosely bound EB from Zn_2 surface. **d**, Potential energy profile of EGD

decomposition on $Zn_2L(OH)_2$ compound. The inset shows the DFT optimized geometries for reactants and intermediates.

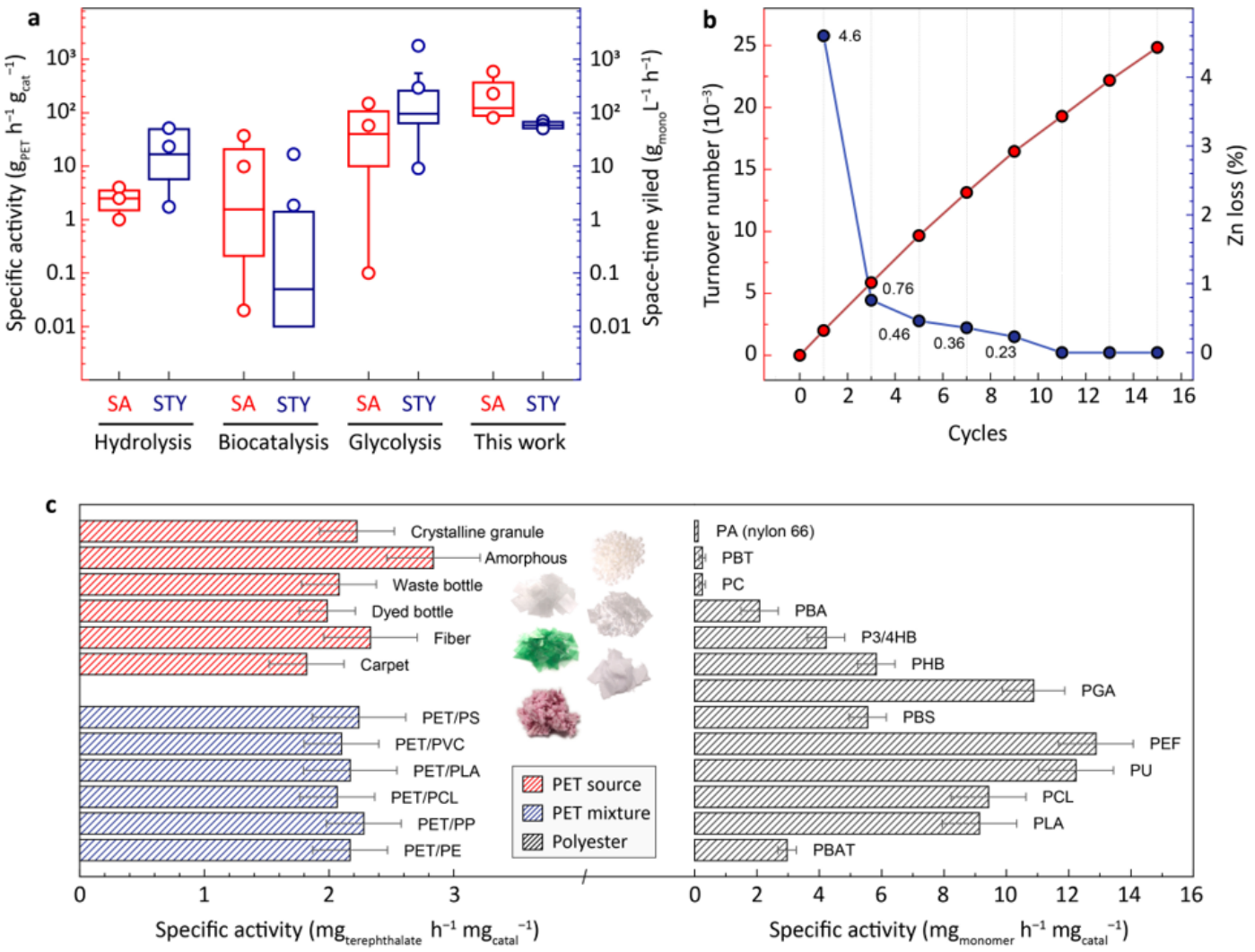

Figure 5

PET recycling over Zn_2/C and substrate scope. a, Comparison of the specific activities (SA, red) and space-time yields (STY, blue) of terephthalate of the alkaline hydrolysis, biocatalysis, glycolysis, and Zn_2/C-catalyzed hydrolysis (data obtained at 90 °C in 50 mL of NaOH aqueous solution (pH 13) containing 50 g of crystalline PET and 5–50 mg of $Zn_2L(NO_3)_2$ supported on carbon, Methods). The production rate of glycolysis was calculated on basis of bis(2-hydroxyethyl) terephthalate. **b**, Recycling and reuse of Zn_2/C in the depolymerization of crystalline PET and the percentage of zinc loss for each cycle as determined by ICP-OES. **c**, The specific activities of Zn_2/C toward different PET sources, PET mixtures, and various polyesters and polyamide at pH 13 and 60 °C. The average specific activities were calculated at 60–80% conversion of polyesters (15% conversion for PA) in 10 mL of NaOH aqueous solution (pH 13) containing 0.32 g of polyesters or polyamide and 2 mg of $Zn_2L(NO_3)_2$ supported on

carbon. Insets show the images of PET crystalline granules, amorphous flakes, clear and dyed bottle flakes, and cloth fibers. All the error bars in this figure represent the standard deviations for three measurements.

Supplementary Files

This is a list of supplementary files associated with this preprint. Click to download.

- PETSI.docx
- ExtendedDataFigs.docx